Rapid Oceanic Response to Tropical Cyclone Oli (2010) over the South Pacific

LUDIVINE ORUBA

Department of Physics, Ecole Normale Supérieure, Paris, France

SERGE PLANES, GILLES SIU, AND YANNICK CHANCERELLE

CRIOBE/USR 3278, CNRS-EPHE-UPVD, Moorea, Polynésie Française

EMMANUEL DORMY

Department of Mathematics and Applications, CNRS UMR 8553, Ecole Normale Supérieure, Paris, France

(Manuscript received 13 September 2016, in final form 13 December 2016)

ABSTRACT

The effect of Tropical Cyclone Oli (2010) on the ocean is investigated using a variety of measurements. In situ temperature measurements on the cyclone track are available via the Centre de Recherches Insulaires et Observatoire de l'Environnement (CRIOBE) array of probes. This reflects an extreme fluctuation of the temperature some 18 h after the cyclone, lasting only 12 h and exceeding 3°C in amplitude. This study interprets this extreme fluctuation in terms of enhanced mixing associated with the time-dependent inertial currents due to the cyclonic winds. The authors show, using Lagrangian simulations, that this rapid event is compatible with the severe length-scale shortening observed in Lagrangian simulations.

1. Introduction

Tropical cyclones (TCs) are among the most deadly and destructive natural disasters on Earth. Despite their high societal impact and the numerous investigations on TCs, their dynamics and their interaction with the upper ocean still present a large number of fascinating and unresolved issues (e.g., Emanuel 2003; Wang 2012).

French Polynesia is not generally regarded as a cyclone-prone area, despite the warm surrounding ocean, because of the relatively strong wind shear over the troposphere, which provides an unfavorable environment to TC genesis. The western South Pacific area is comparably more favorable to TCs. The ENSO (El Niño Southern Oscillation,) however, modifies this picture. In the central and eastern South Pacific Ocean, the hurricane season is typically more active during El Niño both because of an increase of the SST (Basher and Zheng 1995) and the expanded area of low vertical wind shear (Dowdy et al. 2012).

A moderate El Niño episode occurred between June 2009 and May 2010. Tropical phenomena thus developed farther to the east in the South Pacific basin. Among them, TC Oli is one of the most devastating cyclones to have hit French Polynesia over the last 30 yr, having forced the evacuation of thousands of people and destroying over 280 houses in the Society and Austral Islands. It was associated a maximum sustained wind of 51 m s^{-1} (over a 10-min period), with wind gusts reaching 75 m s^{-1}, and a minimum pressure at the center of 925 hPa (category 4 on the Saffir–Simpson scale). It lasted from 1 to 7 February 2010 and covered some 5000 km in the South Pacific Ocean. It impacted the island of Tubuai in the Austral Islands on 5 February at 1200 UTC. This island was precisely on TC Oli's track: the eye was reported between 1400 and 1500 UTC. The cyclone had eased to a maximum sustained wind of 40 m s^{-1} (over a 10-min period).

In this paper, we will investigate the effect of Tropical Cyclone Oli on the ocean temperature using a variety of measurements. The cold SST in the wake of tropical cyclones is well known since the 1960s. The dominant processes responsible for the surface cooling induced by TCs have mainly been discussed through case studies based on in situ observations (e.g., Leipper 1967; D'Asaro 2003), satellite observations (e.g., Chiang et al. 2011; Lloyd and Vecchi 2011), and numerical models

Corresponding author e-mail: Emmanuel Dormy, emmanuel.dormy@ens.fr

DOI: 10.1175/JPO-D-16-0205.1

(e.g., Price 1981; Vincent et al. 2012). Three main processes have been highlighted in these studies: air–sea heat exchange, oceanic vertical mixing, and advection. The most important effect is the entrainment of cold water from the thermocline into the mixed layer through vertical mixing (see Price 1981). Both advection and surface heat fluxes have been shown to be of secondary importance in most cases, but they can play a nonnegligible role in some particular cases (e.g., Huang et al. 2009).

2. Observations of the temperature anomaly associated with TC Oli

The Centre de Recherches Insulaires et Observatoire de l'Environnement (CRIOBE), the CNRS Marine Research Station in French Polynesia, has deployed a wide array of 21 temperature probes over the islands of French Polynesia. This network was originally instrumented to study the marine ecosystem [Service d'Observation CORAIL (SO CORAIL)[1]]. It turns out that one of these probes is located at a 14-m depth on the outer reef of the island of Tubuai [23°20.66′S, 149°24.22′W, in the World Geodetic System 1984 (WGS 84)]. This Seabird SBE56 probe thus offers an accurate and reliable in situ measurement of the sea temperature at a 14-m depth, so within the oceanic mixed layer (OML), precisely on the cyclone track, with a temporal resolution of 1 h.

Figure 1a shows the temperature recorded by the CRIOBE probe over a 2-yr period, between 1 February 2009 and 1 February 2011. In addition to the slow seasonal fluctuations, a noticeable feature is the extreme fluctuation to lower temperature (22.7°C) recorded on 6 February between 0600 and 1200 UTC. This rapid fluctuation occurs about 18 h after the eye of Oli has crossed the island of Tubuai (the crossing time is indicated by the vertical gray line on the enlarged panel; Fig. 1c). This fluctuation is described by some 12 consecutive data points; it is well sampled and cannot be attributed to a technical failure. This extreme fluctuation clearly appears associated with TC Oli. Its unusual amplitude can be quantified by subtracting the 7-day running average (red curve in Fig. 1a) from the hourly measurements. The resulting temperature fluctuation (represented in Fig. 1b) exhibits a standard deviation $\sigma = 0.23$°C, and the fluctuation of 6 February corresponds to 13σ, which highlights its nature as an extreme event in the recording.

To further investigate this temperature anomaly, we superimposed in Fig. 1c the value of the daily satellite SST at the location of the probe. We rely here on the Multiscale Ultrahigh Resolution (MUR) level-4 SST product, a 0.011° latitude–longitude gridded dataset developed by NASA JPL. The curves of the temperature measured by the probe and the MUR SST reconstructed at the same location (Fig. 1c) exhibit very similar variations, except for the extreme fluctuation, which is not visible in the MUR SST measurements. The absence of extreme fluctuation on the SST maps suggests a small-scale phenomenon; lower than the resolution of these reconstructions, which is particularly poor during a tropical cyclone.

The SST maps allow us to capture mesoscale variations of the temperature. Figure 2 shows the difference of SST between 29 January and 8 February, which is a way to measure the effect of TC Oli on the SST. We superimposed the trajectory of TC Oli, obtained from the WMO International Best Track Archive for Climate Stewardship (IBTrACS; Knapp et al. 2010).[2] A cold anomaly is visible along the track of the cyclone and over 200 km away from the track. It corresponds to the cold wake of the cyclone, mentioned in section 1. It is here essentially aligned with the cyclone track, and no left-hand side shift is noticeable (see D'Asaro et al. 2014).

3. Physical mechanisms of the SST evolution

We are concerned in this article with the evolution of the temperature in the OML. It will be measured either at the surface (SST) or at a 14-m depth (CRIOBE measurements).

The conservation of heat in the mixed layer is given by the equation

$$\frac{DT}{Dt} = -\frac{Q_0}{\rho_w C_{p_w} h} - \frac{w_e \delta T}{h}, \tag{1}$$

where T corresponds to the temperature in the bulk mixed layer. The left-hand side term is the horizontal Lagrangian derivative (i.e., the Lagrangian derivative at the surface of the ocean). The first term on the right-hand side (rhs) corresponds to variations associated with the turbulent surface heat flux Q_0 (W m^{-2}), which is the sum of the sensible heat flux Q_S and the latent heat flux Q_L. Heat transfer (sensible heat flux) and evaporation (latent heat flux) from the ocean surface providing the source of energy for TCs in the form of heat and moisture. The parameters ρ_w and C_{p_w} correspond to the volumetric mass density and the constant pressure specific heat of salted water, respectively. The second term on the rhs of (1) corresponds to the turbulent entrainment flux at the bottom of the mixed layer associated with its deepening. It involves the temperature difference δT between the mixed

[1] Service d'Observation CORAIL: http://observatoire.criobe.pf.

[2] https://www.ncdc.noaa.gov/ibtracs/.

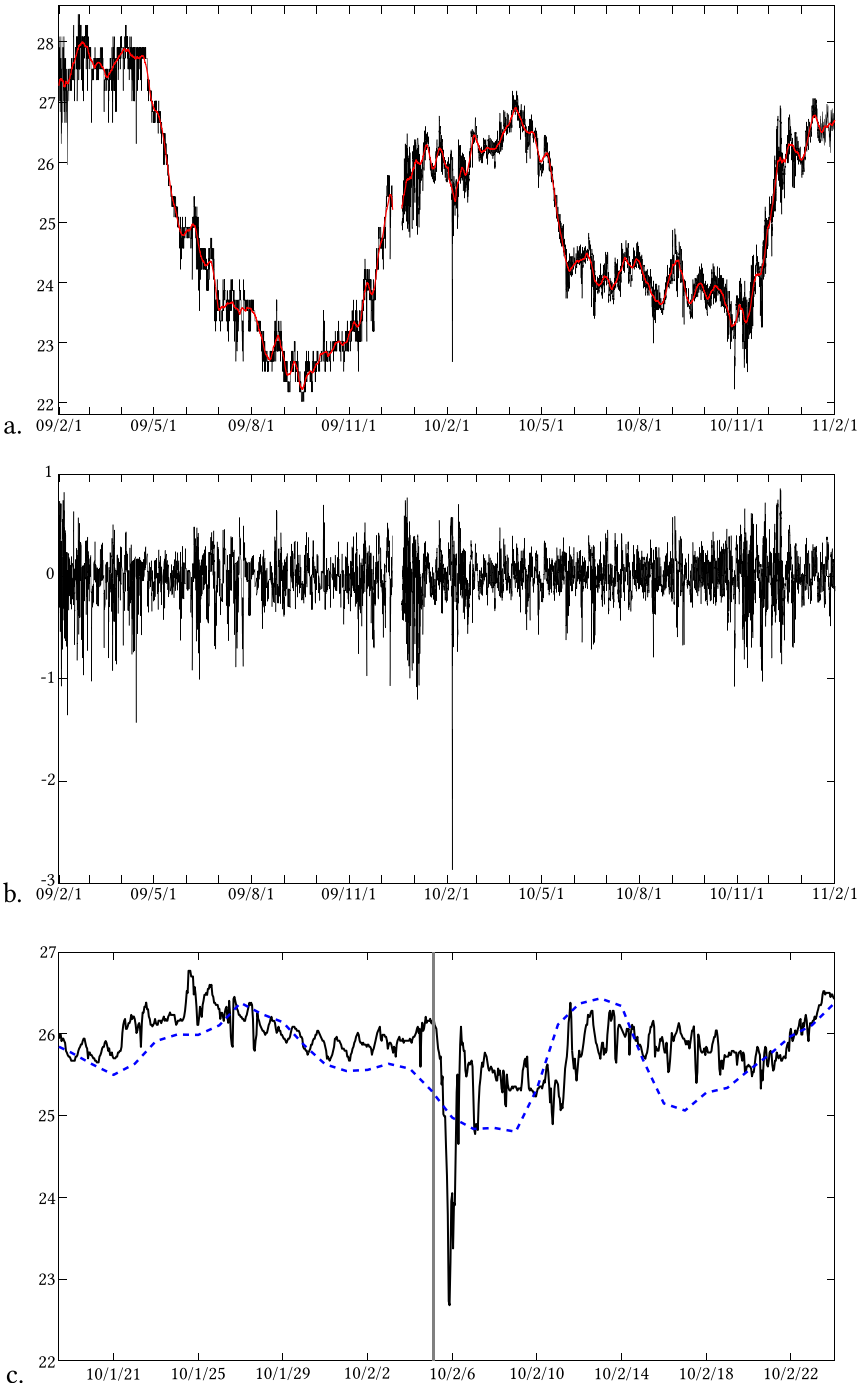

FIG. 1. (a) Time evolution of the temperature (°C) recorded by the CRIOBE probe at a 14-m depth on the outer reef of the island of Tubuai (23°20.66′S, 149°24.22′W) between 1 Feb 2009 and 1 Feb 2011 (black line). The red line corresponds to a 7-day running average. (b) The difference between the temperature and its 7-day running average. (c) An enlarged version of (a) centered on the passage of TC Oli. It combines the temperature measured by the probe (black curve) and the time evolution of the SST reconstruction using satellite data at the same coordinates on a 0.011° grid (blue dashed curve). The vertical gray line indicates the time at which the eye of Oli was over the Tubuai Island. The date format is year/month/day (1200 UTC).

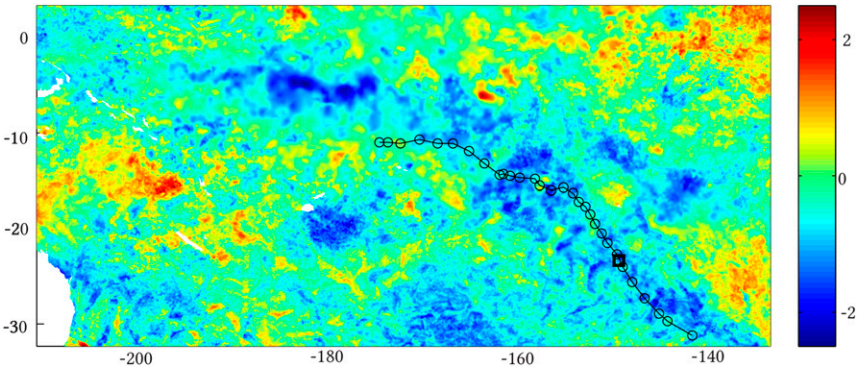

FIG. 2. Map of the difference of MUR SST maps (°C) on 29 Jan and 8 Feb. The location of Tubuai is indicated by a black square. The black curve corresponds to the trajectory of TC Oli (using IBTrACS), from 0600 UTC 29 Jan to 1800 UTC 8 Feb; the dots indicate its position every 6 h.

layer and the thermocline just below the mixed layer and the entrainment velocity w_e, which is defined as

$$w_e = h_t + \nabla \cdot (h\mathbf{u}) \quad \text{if} \quad w_e > 0, \quad \text{and} \tag{2}$$

$$w_e = 0 \quad \text{otherwise}, \tag{3}$$

where h_t corresponds to the time derivative of the mixed layer depth h, and $\mathbf{u}$ denotes the horizontal velocity. The entrainment velocity is an intricate quantity because of its strong dependence on the entrainment parameterization (see Jacob et al. 2000).

a. Contribution of surface heat flux

Heat exchanges between the atmosphere and the ocean can be estimated using the standard bulk aerodynamic formula:

$$Q_S = C_H U \Delta T \rho_a C_{p_a}, \quad \text{and}$$

$$Q_L = C_E U \Delta q \rho_a L_v, \tag{4}$$

where U denotes the wind speed above the air–sea interface, ΔT and Δq are the temperature and specific humidity differences between atmosphere and sea surface, ρ_a is the air density, C_{p_a} is the constant pressure specific heat of air, and L_v is the latent heat of vaporization of water. Conventional bulk models rely on the assumption that the heat flux is proportional to the wind speed over the air–sea surface, and the coefficients C_H and C_E are independent on velocity, temperature, and specific humidity fields. Many studies empirically determined the values of the heat exchange coefficients through experiments (e.g., DeCosmo et al. 1996; Jacob et al. 2000; Fairall et al. 2003; Zhang et al. 2008). Following Jacob et al. (2000), we will use $C_H \simeq 1 \times 10^{-3}$ and $C_E \simeq 1.2 \times 10^{-3}$ and $h = 30$ m.

To get an estimate of the parameters U, ΔT and Δq in (4), we rely on ERA-Interim with 6-h time intervals and a spatial resolution of 0.75° latitude by 0.75° longitude (Dee et al. 2011). The parameter U is estimated using the wind speed field at 10 m above the air–sea interface. The quantity ΔT is computed as the difference between the SST and the temperature at 2 m above the surface, and Δq is computed as the difference between the saturated specific humidity at the sea surface and the near-surface specific humidity at 2 m.

Figure 3 shows the heat fluxes Q_S and Q_L (W m^{-2}) from 2 to 6 February. TC Oli generated positive heat fluxes on both sides of its track. The strongest winds being on the left side of the cyclone (with respect to the cyclone's motion), the flux was enhanced on this side. The latent heat flux dominated the sensible heat flux, which is consistent with earlier studies (e.g., Jacob et al. 2000).

We can estimate the difference of temperature caused by the surface heat flux term in (1) by integrating its effect between 1200 UTC 29 January (t_i) and 1200 UTC 8 February (t_f). It results in

$$\Delta \mathrm{SST}_Q = -\int_{t_i}^{t_f} \left(\frac{Q_s + Q_L}{\rho_w C_{p_w} h} \right) dt. \tag{5}$$

This integral can be estimated using fluxes sampled with 6-h time intervals from ERA-Interim. It is represented in Fig. 4. Comparing Fig. 2 with Fig. 4 reveals that the heat fluxes account for the decrease of temperature on both sides of the cyclone's track. It, however, does not account for the cold signature along the track of the cyclone. Similar observations have been reported in earlier case studies (e.g., Morey et al. 2006).

b. Vertical entrainment contribution

Let us now turn to the second term on the right-hand side of (1), which stems from the upwelling associated with the conservation of mass. The vertical upwelling is

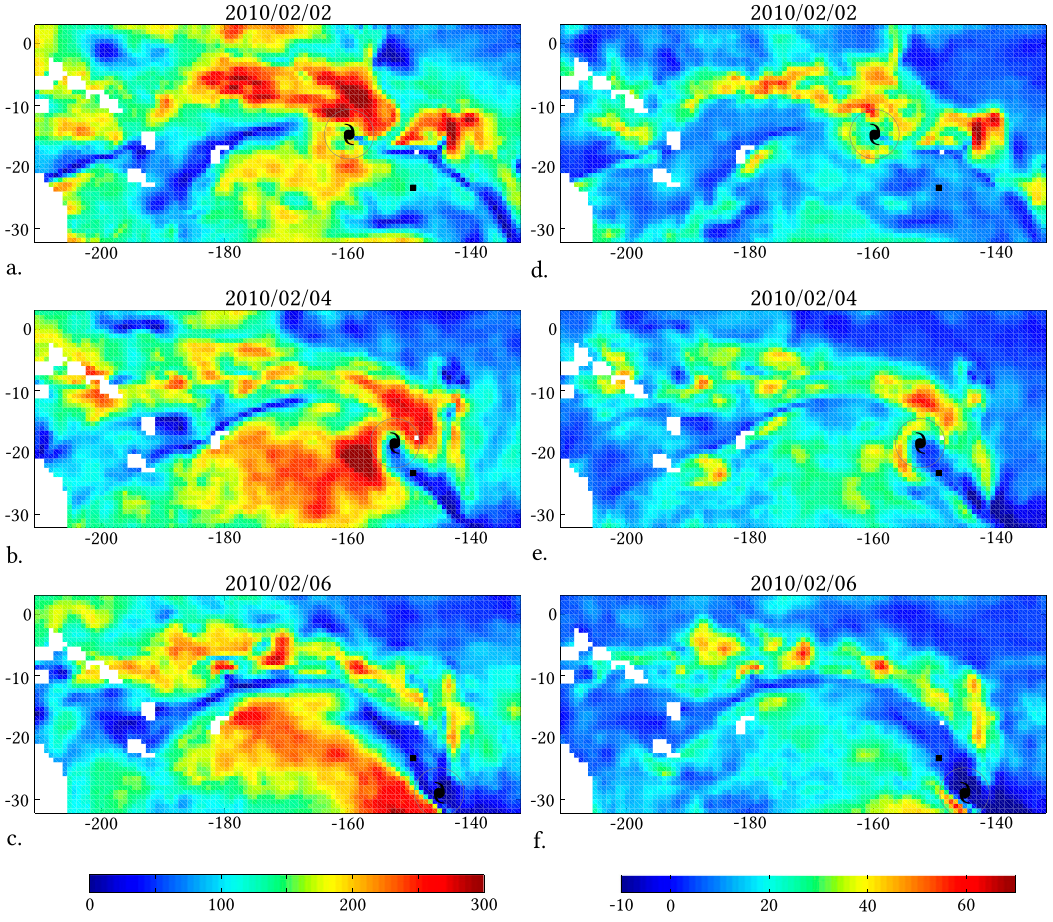

FIG. 3. Heat fluxes (a)–(c) Q_L and (d)–(f) Q_S (W m^{-2}) from 1200 UTC 2 Feb to 1200 UTC 6 Feb, with their respective color codes. The location of Tubuai is indicated by the black square. The symbol indicates the location of the center of TC Oli at 1200 UTC, and the gray circle indicates the 400-km radius.

known to be associated with shear instabilities (e.g., Price 1981; Shay 2010; Hormann et al. 2014) across the base of the mixed layer. The resulting vertical entrainment provides a sink term for (1). While the precise amplitude of this term is difficult to accurately quantify [see Jacob et al. (2000) for a discussion], typical estimates for the total vertical velocity are about 510 cm s^{-1} (e.g., Jullien et al. 2012). Such velocities can account for

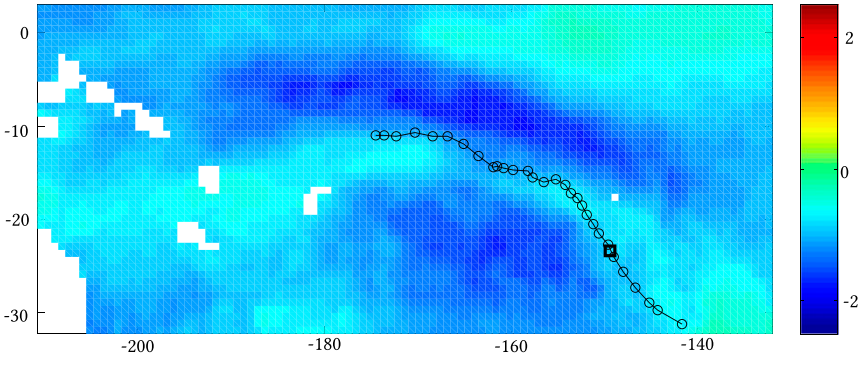

FIG. 4. The reconstructed ΔSST_Q (°C) between 1200 UTC 29 Jan and 1200 UTC 8 Feb using heat fluxes from ERA-Interim [see (5)]. The symbols are the same as in Fig. 2.

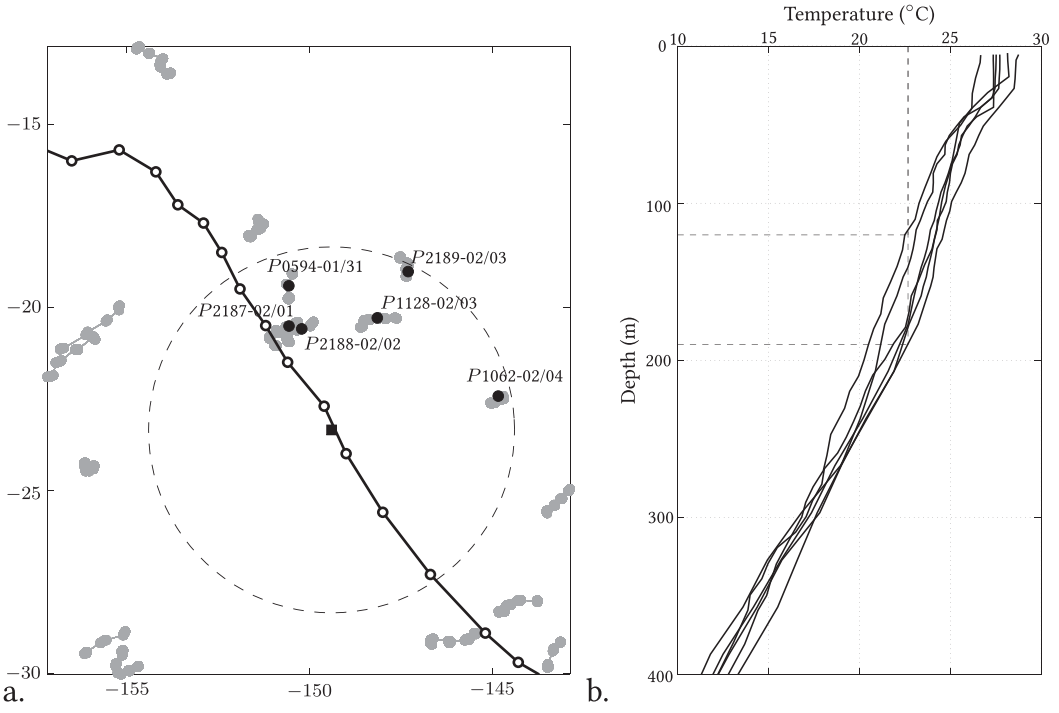

FIG. 5. (a) Map of the trajectories of Argo floats in the area around Tubuai during January and February 2010 (gray dots). The floats evolving within a 500-km range of the island of Tubuai (dashed circle) a few days before TC Oli are highlighted by a black dot. (b) The corresponding vertical profiles of temperature. The black line in (a) corresponds to the trajectory of Oli, the white dots to its position every 6 h. The dashed lines in (b) indicate the range of depth corresponding to the lowest $T_{min} = 22.7$°C temperature measured by the CRIOBE probe in Tubuai on 6 February.

the decrease in temperature along the track of the cyclone (i.e., the cold wake) as observed in Fig. 2. This has been well documented in numerous earlier studies (e.g., Chiang et al. 2011; Vincent et al. 2012; D'Asaro et al. 2014). This estimation is further complicated by nonlinear effects (see Greatbatch 1983), which depend on the storm speed (see Zedler 2009).

It is, however, important to ponder on the mechanisms to account for the very rapid cold event recorded by the CRIOBE probe. It cannot be explained by the entrainment term. The contribution of this term to temperature variations can indeed be further constrained using the vertical temperature profiles measured in the ocean, such as the global ocean temperature measurements performed by the Array for Real-Time Geostrophic Oceanography (Argo; Roemmich and Owens 2000) floats. A total of 3843 floats are currently active all over the globe, each float undergoing a 10-day cycle between surface and 2000-m depth. They provide useful in situ data on the ocean response to TCs (e.g., Fu et al. 2014), but their cycle duration (10 days) and the drift they undergo during this cycle (50–200 km) are limiting factors (see Park et al. 2011). Temperature measurements operated by the CRIOBE thus offer the most useful, high-accuracy, fixed-point data to complement the Argo profiling floats.

Figure 5a shows the trajectory of Argo floats near the island of Tubuai during January and February 2010. We identified six probes evolving within a 500-km range of Tubuai a few days before TC Oli. The corresponding vertical temperature profiles are gathered in Fig. 5a. On these profiles, the slope of the thermocline was similar. The thickness of the OML was about 30 m [consistent with the value chosen to estimate the heat fluxes in (1)]. At the base of the OML, thermal stratification was rather weak; this is consistent with a strong entrainment and the formation of the cold wake visible in Fig. 2 (see Shay 2010).

We now aim at understanding the origin of the rapid cold event ($T_{min} = 22.7$°C) measured by the CRIOBE probe in Tubuai on 6 February at about 0900 UTC. In Fig. 5b, this low temperature is reached at a depth d ranging from 120 to 190 m depending on the location. The time interval between the arrival time of TC Oli in Tubuai (at 1200 UTC on 5 February) and the measurement of T_{min} by the CRIOBE probe (at 0900 UTC 6 February) is $\Delta t = 21$ h. A conservative estimate of the vertical advection velocity w required to advect cold water from depth d over the time interval Δt ranges

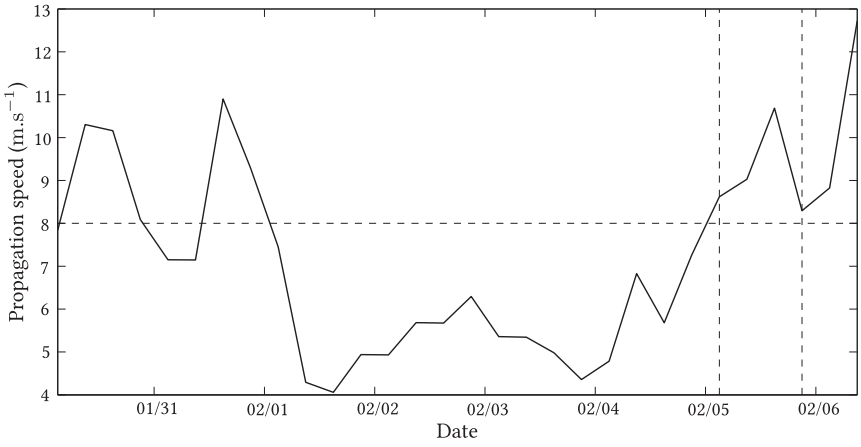

FIG. 6. Translational speed of TC Oli with time based on IBTrACS data. The vertical lines respectively indicate the passage of the eye over Tubuai and the date of the cold extreme event on the CRIOBE recording (dates are indicated at 1200 UTC each day). The 8 m s^{-1} threshold is highlighted by the horizontal dashed line.

between 0.16 and 0.25 cm s^{-1}. This assumes advection in a straight path and does not take into account mixing. It is thus a very conservative estimate. Such values are at least one order of magnitude too large compared to standard upwelling estimates under TCs (e.g., Jullien et al. 2012). The extreme variation recorded by the CRIOBE probe therefore is very unlikely to be associated with vertical entrainment, since it would require unrealistically large vertical velocities.

It should be stressed that TC Oli was rapidly moving as it crossed the island of Tubuai, with a translational speed larger than 8 m s^{-1} (see Fig. 6). It is well known (Price 1981) that for a slow-moving cyclone (translation speed < 4 m s^{-1}) strong upwelling can occur. This was documented for TC Kai-Tak in the South China Sea in 2000. Immediately after TC Kai-Tak, a cold wake characterized by a drop in SST as large as 9°C was measured (Lin et al. 2003; Chiang et al. 2011). The situation is clearly different for TC Oli, which was rapidly moving. Besides, the cold wake behind TC Kai-Tak corresponded to a spatial extension comparable to the radius of maximum wind (RMW; see Lin et al. 2003). This thus significantly differs from the situation of TC Oli, for which SST measurements (Fig. 2) show that the large-scale cold wake corresponded to a drop of 2°C. Moreover, the large-scale (comparable with the RMW) temperature anomaly induced by TC Kai-Tak lasted several days (see Lin et al. 2003), so much longer than the rapid and extreme temperature drop recorded by the CRIOBE probe. This last event must thus be associated with a smaller horizontal length scale.

Smaller structures could possibly result from coastal upwelling. While the seafloor near Tubuai is about 6000 m deep, it is worth pondering the effect of the volcanic dome that forms the island. The typical width of the island of Tubuai at the surface is about 8 km, but the volcano obviously widens with depth. At a depth of 120–190 m, bathymetry data (ETOPO1 global relief model; Amante and Eakins 2009) indicate that its typical width has increased to about 16 km. Such typical scales might be associated with rapid variations (as recorded on the CRIOBE probe). However, several studies on coastal upwelling (with currents of comparable strength as the ones in this study) indicate that these flows are also one order of magnitude too weak to account for the observed variations (see Csanady 2001; Zamudio et al. 2010).

In the absence of the physical mechanism to provide the rapid and localized transport needed to explain the CRIOBE data via vertical advection, we should now consider the effects of horizontal Lagrangian transport.

c. *Horizontal Lagrangian transport*

It is known since Arnold (1965) that large-scale smooth flows can yield Lagrangian chaos. Arnold, followed by Henon (1966), showed that an analytical three-dimensional Beltrami flow (known today as the ABC flow) had chaotic trajectories. The velocity field produces chaotic advection of a passive scalar, at least in part of the domain, which will, in the presence of a finite diffusivity, result in enhanced mixing (e.g., Ottino 1989). This chaotic mixing does not occur in a steady incompressible two-dimensional flow, as all trajectories are closed lines (isovalues of the streamfunction). Of course, such is not the case with mesoscale currents, which involve time dependence as well as a vertical component (e.g., Samelson 1992; Muller and Garrett 2002). Tropical Cyclone Oli, however, stirred the ocean

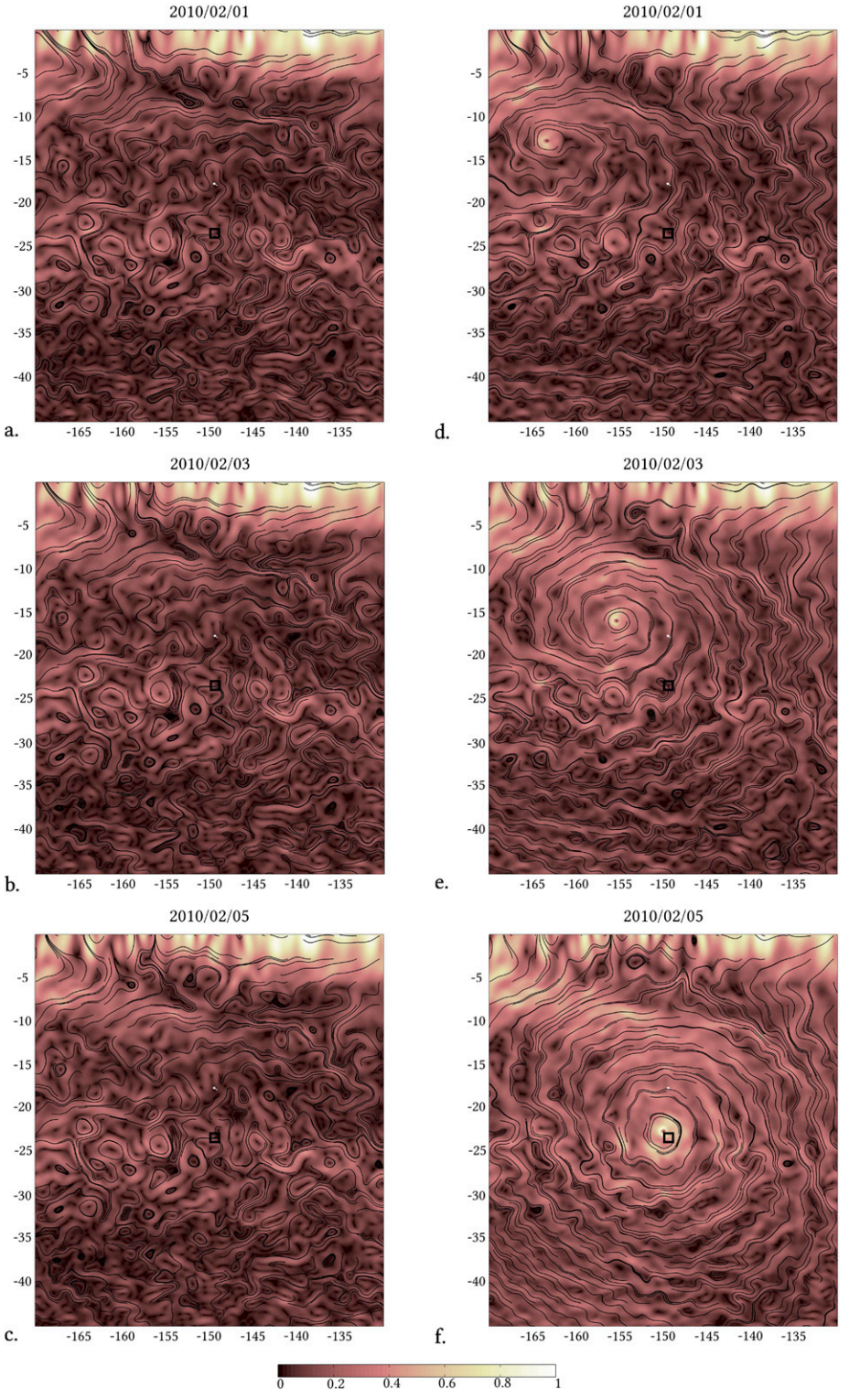

FIG. 7. (left) Instantaneous streamlines of the mesoscale currents as reconstructed from the OSCAR data and (right) including a model of inertial currents driven by the TC winds.

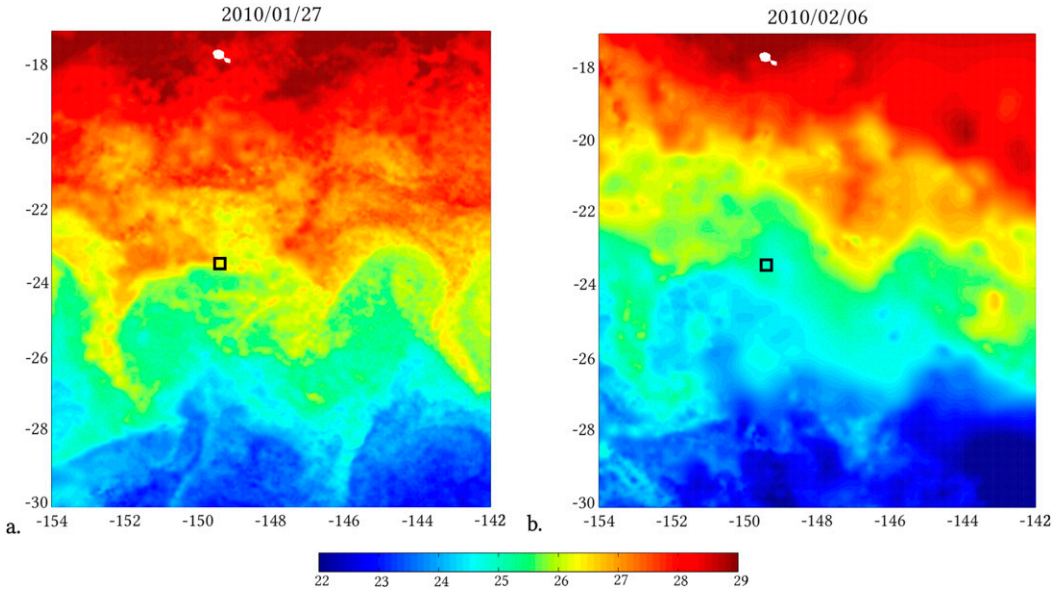

FIG. 8. SST maps as provided by the MUR level-4 SST product on (a) 27 Jan and (b) 6 Feb.

over a typical period of 10 days; over such a short period, the mesoscale flow in this part of the South Pacific can be considered nearly two-dimensional and stationary.

Whereas 2D steady flows cannot result in chaotic mixing, time-dependent 2D flows can achieve this (e.g., Ottino 1989). Early prototypes of such chaotic mixing were constructed on the basis of time-dependent vortices (e.g., Aref 1984; Khakhar et al. 1986). We want to investigate whether the interaction of rapidly varying inertial currents, due to the tropical storm, with the mesoscale circulation can result in enhanced stretching, which would quickly form small-scale filaments. The inertial currents driven by the tropical cyclone will take the form of a rapidly drifting large-scale vortex. This time dependence is reminiscent of flows such as the blinking vortex of Aref (1984). The enhanced stretching associated with such flows could account for the observed small-scale cold current in the CRIOBE data.

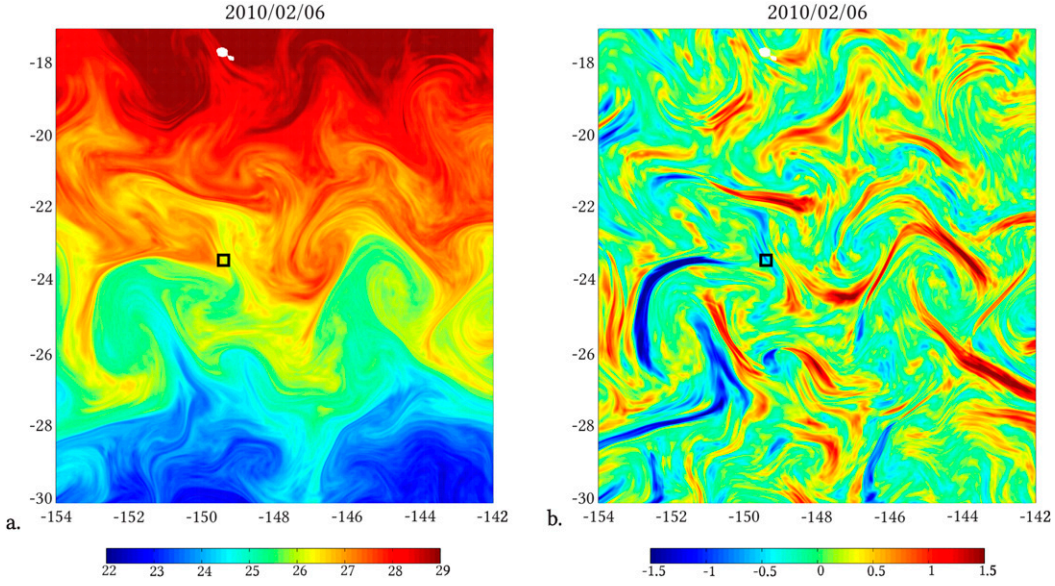

FIG. 9. (a) SST map on 6 February, as reconstructed using a purely Lagrangian advection scheme. (b) Temperature perturbation induced by the tropical cyclone on 6 Feb.

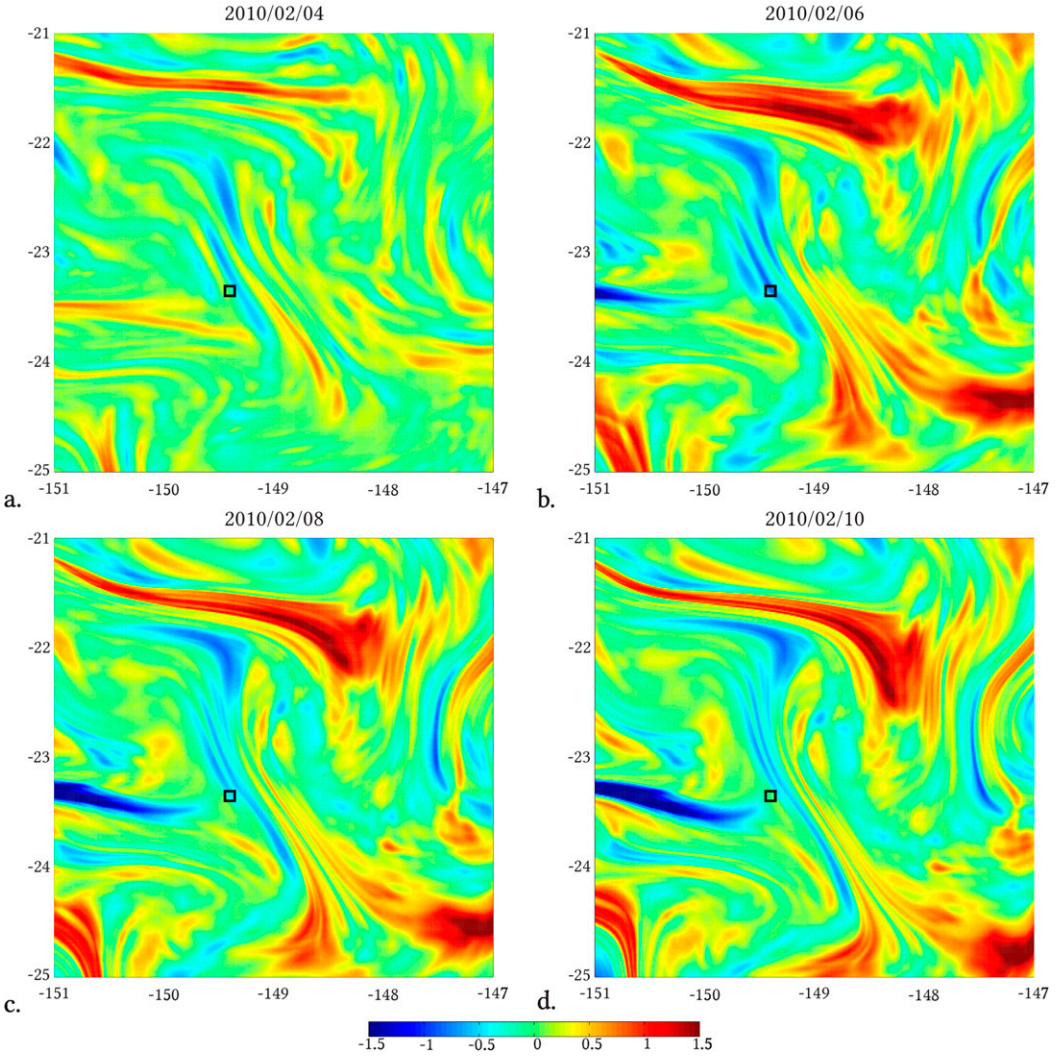

FIG. 10. Time evolution of the temperature perturbation induced by the tropical cyclone on (a) 4, (b) 6, (c) 8, and (d) 10 Feb 2010.

The left-hand side of (1) can be rewritten as

$$\frac{DT}{Dt} \equiv \frac{\partial T}{\partial t} + \mathbf{u} \cdot \nabla T, \tag{6}$$

and we now need to model the horizontal flow $\mathbf{u}$.

To compute the horizontal advection of temperature via mesoscale currents, we rely on the Ocean Surface Current Analyses–Real Time (OSCAR) product. The corresponding near-surface currents are estimated on a $1/3^\circ \times 1/3^\circ$ grid with a 5-day resolution through a simplified diagnostic model of the surface circulation, combining satellite and in situ measurements of sea surface height, surface vector wind, and sea surface temperature.

We present OSCAR current maps reconstructed over the period of TC Oli in Figs. 7a, 7b, and 7c. The nearly two-dimensional characteristic of the current is clearly visible. These currents evolve on a slow time scale, typically of the order of a month. So though their reconstruction is obviously seriously complicated at the time of the tropical storm, we can rely on this model to provide a reasonably accurate reconstruction of the mesoscale currents over a period of a few days. There is no signature of TC Oli on these currents, as the satellite data are scarce over the period of the cyclone.

To account for inertial currents associated with TC Oli, we need to rely on a wind model for the TC. Using winds from the ERA-Interim data introduces known limitations. Low-atmospheric resolution is known to smooth out the maximum winds and to overestimate the RMW (e.g., Murakami 2014; Jourdain et al. 2014). Rather than using ERA-Interim wind profiles, we thus

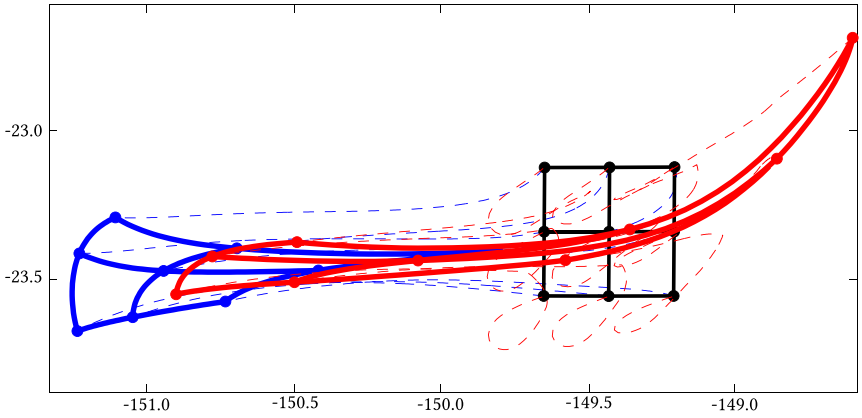

FIG. 11. Enhanced stretching associated with cyclonic inertial currents. The blue curves indicate the preimage of a square of size 0.44° centered on the island of Tubuai on 6 Feb (black lines), 10 days before the extreme fluctuation. The red curves indicate the corresponding preimage taking into account the presence of inertial currents. Dashed lines correspond to the trajectories of the edges.

rely on an analytical vortex profile to represent the radial structure of the TC primary circulation. We rely here on a modified Rankine vortex (e.g., Hughes 1952)

$$\begin{aligned} v &= v_m \frac{r}{r_m} \quad \text{for} \quad r < r_m, \\ v &= v_m \left(\frac{r_m}{r}\right)^{\alpha} \quad \text{for} \quad r > r_m, \end{aligned} \tag{7}$$

where v_m is the maximum winds, r_m is the RMW, and α is a scaling parameter that adjusts the profile shape. Because of the frictional losses of angular momentum, $\alpha < 1$. In our study, α is set, as in Riehl (1963) and Pearce (1993), to $\alpha = 1/2$. The RMW is set to $r_m = 40$ km, which coincides with measurements for TC Oli. We use the position and the maximum wind speed of Oli in the IBTrACs database; they will be interpolated in the numerical algorithm in between these data points (available every 6 h).

For strong winds, inertial currents are nearly aligned with the wind, with a ratio of wind velocity to surface currents velocity of 2% (see Chang et al. 2012), consistent with $\rho_a v_a^2 \simeq \rho_w v_w^2$. Such strong wind-driven inertial currents can be superimposed to the time-averaged mesoscale currents. The resulting combined currents are represented in Figs. 7d, 7e, and 7f. They are of comparable magnitudes as the OSCAR currents (Figs. 7a,b,c) but do vary on a much shorter time scale, owing to the rapid displacement of the cyclone.

To model the effects of the cyclone on the SST, we need to define some initial conditions. We set the initial temperature map to be that of 27 January. This choice is driven by several considerations. First, the SST map for this day is of good accuracy (the moderate amount of cloud allowed reliable measurements); it is represented in Fig. 8a. Second, the time lag between 27 January and 6 February (when the cold current is measured over Tubuai) corresponds to 10 days. This period of time corresponds approximately to the turnover time of mesoscale eddies and is short enough to consider pure Lagrangian advection at the resolution of the SST maps (0.011°). Figure 8b represents the SST as available from the MUR SST data on 6 February. The apparent lack of resolution on this map results from the presence of massive storm clouds.

The initial temperature map (27 January; Fig. 5a) can be advected to 6 February using a nondiffusive, purely Lagrangian reconstruction scheme. This results in Fig. 9a. Very finescale structures (of submesoscale) are clearly visible on this map. Besides, a small-scale cold current is visible near the island of Tubuai (indicated by a black square). Its width approaches the resolution of our maps (set to that of the SST map, which served as initial condition, i.e., 0.011°), and it could be even colder and of even smaller scale in practice.

To quantify the role of the inertial currents associated with TC Oli on this temperature map, we represent in Fig. 9b the difference of the map computed with our complete current reconstruction (including inertial currents) to that due to the slowly varying mesoscale circulation only.

The first striking feature of this map is the small filamentary structure of the temperature fluctuations associated with the TC. The second interesting feature, in order to compare with the CRIOBE data, is the presence of narrow cold temperature perturbations around the island of Tubuai on 6 February.

An enlarged representation of the cold perturbation is represented in Fig. 10. This figure highlights a natural consequence of the filamentary structures of temperature

perturbations associated with the TC: their rapid variation in time at a given position (here the island of Tubuai).

To highlight the enhanced stretching, we computed in Fig. 11 a preimage of a square of size 0.44° centered on Tubuai, that is, the initial position (on 27 January) of the patch, which will be advected by the time-dependent current flow to the square on 6 February. In the absence of cyclone (blue patch), some stretching is evident, but the whole patch is advected from the southwest of Tubuai. In the case of the simulation including inertial currents, not only is the stretching very significantly enhanced, but the position of the original patch (in red), which will be advected to Tubuai, now comes both from the southwest and from the northeast. This situation, characteristic of hyperbolic trajectories, accounts for the very short length scales observed in Fig. 10. Indeed, the direction of the fine temperature perturbation structures in Fig. 10 are aligned with the direction of strong stretching and are orthogonal to the contracting direction highlighted in Fig. 11.

4. Discussion

While chaotic mixing is known to occur in the ocean (e.g., Muller and Garrett 2002; Berti and Lapeyre 2014), we have shown that the rapidly varying inertial currents associated with a tropical cyclone significantly enhance the stretching and yield the rapid formation of fine filaments of temperature perturbations, which are rapidly elongated, over the lifetime of the cyclone. The Lagrangian advection is only considered here over one mesoscale eddy turnover time. This is too short to assess Lagrangian chaos (tools such as Poincaré cross sections cannot be used over this short range); however, length-scale shortening is evident from Figs. 9 to 10, suggestive of the presence of enhanced stretching near the island of Tubuai.

Our reconstructed SST via Lagrangian advection does not claim to be exact. It is important to bear in mind the limitations. These concern in particular the mesoscale currents model, the initial (on 27 January 2010) map of SST with finite resolution, and the model of inertial currents driven by the storm wind.

What we have highlighted with this study, however, is the strong enhancement of the stretching properties of the surface flow during the time of the cyclone. It is not due to stronger currents than usual (the order of magnitude of the currents is not significantly altered) but rather to their rapid time dependence.

The rapidly varying currents provide very elongated filaments of temperature perturbations. In our model, the typical length of the temperature perturbation is much smaller than the characteristic scale of the flow. The stretching and orientation of thermal structures are driven by the velocity gradients. This enhanced stretching is compatible with the extreme rapid fluctuation of the CRIOBE data recorded in Tubuai shortly following TC Oli. Higher-resolution satellite SST maps will open new perspectives for a better description of such very finescale structures.

Acknowledgments. This project was made possible using data provided by the Service d'Observation "CORAIL" mainly funded by the INSU together with the Ministry for Environment and IFRECOR. It was partially supported by the French National Center for Research under the interdisciplinary Grant Inphyniti/MI/CNRS (awarded to L. Oruba and E. Dormy). The Group for High Resolution Sea Surface Temperature (GHRSST) Multiscale Ultrahigh Resolution (MUR) SST data were obtained from the NASA EOSDIS Physical Oceanography Distributed Active Archive Center (PO.DAAC) at the Jet Propulsion Laboratory, Pasadena, CA (http://dx.doi.org/10.5067/GHGMR-4FJ01). The Argo data were collected and made freely available by the International Argo Program and the national programs that contribute to it (http://www.argo.ucsd.edu; http://argo.jcommops.org). The Argo Program is part of the Global Ocean Observing System. The OSCAR data were obtained from JPL Physical Oceanography DAAC and developed by ESR.

REFERENCES

Amante, C., and B. Eakins, 2009: ETOPO1 1 arc-minute global relief model: Procedures, data sources and analysis. NOAA Tech. Memo. NESDIS NGDC-24, 25 pp. [Available online at https://www.ngdc.noaa.gov/mgg/global/relief/ETOPO1/docs/ETOPO1.pdf.]

Aref, H., 1984: Stirring by chaotic advection. *J. Fluid Mech.*, **143**, 1–21, doi:10.1017/S0022112084001233.

Arnold, V., 1965: Sur la topologie des écoulements stationnaires des fluides parfaits. *C. R. Acad. Sci. Paris*, **261**, 17–20.

Basher, R. E., and X. Zheng, 1995: Tropical cyclones in the southwest Pacific: Spatial patterns and relationships to Southern Oscillation and sea surface temperature. *J. Climate*, **8**, 1249–1260, doi:10.1175/1520-0442(1995)008<1249:TCITSP>2.0.CO;2.

Berti, S., and G. Lapeyre, 2014: Lagrangian reconstructions of temperature and velocity in a model of surface ocean turbulence. *Ocean Modell.*, **76**, 59–71, doi:10.1016/j.ocemod.2014.02.003.

Chang, Y.-C., G.-Y. Chen, R.-S. Tseng, L. R. Centurioni, and P. C. Chu, 2012: Observed near-surface currents under high wind speeds. *J. Geophys. Res.*, **117**, C11026, doi:10.1029/2012JC007996.

Chiang, T. L., C. R. Wu, and L. Y. Oey, 2011: Typhoon Kai-Tak: An ocean's perfect storm. *J. Phys. Oceanogr.*, **41**, 221–233, doi:10.1175/2010JPO4518.1.

Csanady, G. T., 2001: *Air-Sea Interaction: Laws and Mechanisms*. Cambridge University Press, 239 pp.

D'Asaro, E. A., 2003: The ocean boundary layer below Hurricane Dennis. *J. Phys. Oceanogr.*, **33**, 561–579, doi:10.1175/1520-0485(2003)033<0561:TOBLBH>2.0.CO;2.

——, and Coauthors, 2014: Impact of typhoons on the ocean in the Pacific. *Bull. Amer. Meteor. Soc.*, **95**, 1405–1418, doi:10.1175/BAMS-D-12-00104.1.

DeCosmo, J., K. B. Katsaros, S. D. Smith, R. J. Anderson, W. A. Oost, K. Bumke, and H. Chadwick, 1996: Air-sea exchange of water vapor and sensible heat: The Humidity Exchange over the Sea (HEXOS) results. *J. Geophys. Res.*, **101**, 12 001–12 016, doi:10.1029/95JC03796.

Dee, D. P., and Coauthors, 2011: The ERA-Interim reanalysis: Configuration and performance of the data assimilation system. *Quart. J. Roy. Meteor. Soc.*, **137**, 553–597, doi:10.1002/qj.828.

Dowdy, A. J., L. Qi, and D. Jones, 2012: Tropical cyclone climatology of the South Pacific Ocean and its relationship to El Nino–Southern Oscillation. *J. Climate*, **25**, 6108–6122, doi:10.1175/JCLI-D-11-00647.1.

Emanuel, K., 2003: Tropical cyclones. *Annu. Rev. Earth Planet. Sci.*, **31**, 75–104, doi:10.1146/annurev.earth.31.100901.141259.

Fairall, C. W., E. F. Bradley, J. E. Hare, A. A. Grachev, and J. B. Edson, 2003: Bulk parameterization of air–sea fluxes: Updates and verification for the COARE algorithm. *J. Climate*, **16**, 571–591, doi:10.1175/1520-0442(2003)016<0571:BPOASF>2.0.CO;2.

Fu, H., X. Wang, P. C. Chu, X. Zhang, G. Han, and W. Li, 2014: Tropical cyclone footprint in the ocean mixed layer observed by Argo in the northwest Pacific. *J. Geophys. Res. Oceans*, **119**, 8078–8092, doi:10.1002/2014JC010316.

Greatbatch, R. J., 1983: On the response of the ocean to a moving storm: The nonlinear dynamics. *J. Phys. Oceanogr.*, **13**, 357–367, doi:10.1175/1520-0485(1983)013<0357:OTROTO>2.0.CO;2.

Henon, M., 1966: Sur la topologie des lignes de courant dans un cas particulier. *C. R. Acad. Sci. Paris*, **262**, 312–314.

Hormann, V., L. R. Centurioni, L. Rainville, C. M. Lee, and L. J. Braasch, 2014: Response of upper ocean currents to Typhoon Fanapi. *Geophys. Res. Lett.*, **41**, 3995–4003, doi:10.1002/2014GL060317.

Huang, P., T. B. Sanford, and J. Imberger, 2009: Heat and turbulent kinetic energy budgets for surface layer cooling induced by the passage of Hurricane Frances (2004). *J. Geophys. Res*, **114**, C12023, doi:10.1029/2009JC005603.

Hughes, L. A., 1952: On the low-level wind structure of tropical storms. *J. Meteor.*, **9**, 422–428, doi:10.1175/1520-0469(1952)009<0422:OTLLSO>2.0.CO;2.

Jacob, S. D., L. K. Shay, and A. J. Mariano, 2000: The 3D oceanic mixed layer response to Hurricane Gilbert. *J. Phys. Oceanogr.*, **30**, 1407–1429, doi:10.1175/1520-0485(2000)030<1407:TOMLRT>2.0.CO;2.

Jourdain, N. C., B. Barnier, N. Ferry, J. Vialard, C. E. Menkes, M. Lengaigne, and L. Parent, 2014: Tropical cyclones in two atmospheric (re)analyses and their response in two oceanic reanalyses. *Ocean Modell.*, **73**, 108–122, doi:10.1016/j.ocemod.2013.10.007.

Jullien, S., and Coauthors, 2012: Impact of tropical cyclones on the heat budget of the South Pacific Ocean. *J. Phys. Oceanogr.*, **42**, 1882–1906, doi:10.1175/JPO-D-11-0133.1.

Khakhar, D. V., H. Rising, and J. M. Ottino, 1986: An analysis of chaotic mixing in two model systems. *J. Fluid Mech.*, **172**, 419–451, doi:10.1017/S0022112086001805.

Knapp, K. R., M. C. Kruk, D. H. Levinson, H. J. Diamond, and C. J. Neumann, 2010: The International Best Track Archive for Climate Stewardship (IBTrACS): Unifying tropical cyclone best track data. *Bull. Amer. Meteor. Soc.*, **91**, 363–376, doi:10.1175/2009BAMS2755.1.

Leipper, D. F., 1967: Observed ocean conditions and Hurricane Hilda, 1964. *J. Atmos. Sci.*, **24**, 182–196, doi:10.1175/1520-0469(1967)024<0182:OOCAHH>2.0.CO;2.

Lin, I., and Coauthors, 2003: New evidence for enhanced ocean primary production triggered by tropical cyclone. *Geophys. Res. Lett.*, **30**, 1718, doi:10.1029/2003GL017141.

Lloyd, I. D., and G. A. Vecchi, 2011: Observational evidence of oceanic controls on hurricane intensity. *J. Climate*, **24**, 1138–1153, doi:10.1175/2010JCLI3763.1.

Morey, S. L., M. A. Bourassa, D. S. Dukhovskoy, and J. J. O'Brien, 2006: Modeling studies of the upper ocean response to a tropical cyclone. *Ocean Dyn.*, **56**, 594–606, doi:10.1007/s10236-006-0085-y.

Muller, P., and C. Garrett, 2002: From stirring to mixing in a stratified ocean. *Oceanography*, **15**, 12–19, doi:10.5670/oceanog.2002.10.

Murakami, H., 2014: Tropical cyclones in reanalysis data sets. *Geophys. Res. Lett.*, **41**, 2133–2141, doi:10.1002/2014GL059519.

Ottino, J. M., 1989: *The Kinematics of Mixing: Stretching, Chaos, and Transport*. Cambridge University Press, 364 pp.

Park, J. J., Y.-O. Kwon, and J. F. Price, 2011: Argo array observation of ocean heat content changes induced by tropical cyclones in the North Pacific. *J. Geophys. Res.*, **116**, C12025, doi:10.1029/2011JC007165.

Pearce, R. P., 1993: A critical review of progress in tropical cyclone physics including experimentation with numerical models. *Proc. ICSU/WMO Int. Symp. on Tropical Disasters*, Beijing, China, ICSU, 45–59.

Price, J., 1981: Upper ocean response to a hurricane. *J. Phys. Oceanogr.*, **11**, 153–175, doi:10.1175/1520-0485(1981)011<0153:UORTAH>2.0.CO;2.

Riehl, H., 1963: Some relations between wind and thermal structure of steady state hurricanes. *J. Amer. Sci.*, **20**, 276–287, doi:10.1175/1520-0469(1963)020<0276:SRBWAT>2.0.CO;2.

Roemmich, D., and W. B. Owens, 2000: The Argo project: Global ocean observations for understanding and prediction of climate variability. *Oceanography*, **13**, 45–50, doi:10.5670/oceanog.2000.33.

Samelson, R. M., 1992: Fluid exchange across a meandering jet. *J. Phys. Oceanogr.*, **22**, 431–440, doi:10.1175/1520-0485(1992)022<0431:FEAAMJ>2.0.CO;2.

Shay, L. K., 2010: Air-sea interactions in tropical cyclones. *Global Perspectives on Tropical Cyclones: From Science to Mitigation*, J. C. L. Chan and J. D. Kepert, Eds., Vol. 4, World Scientific, 93–131.

Vincent, E. M., M. Lengaigne, G. Madec, J. Vialard, G. Samson, N. Jourdaina, C. E. Menkes, and S. Jullien, 2012: Processes setting the characteristics of sea surface cooling induced by tropical cyclones. *J. Geophys. Res.*, **117**, C02020, doi:10.1029/2011JC007396.

Wang, Y., 2012: Recent research progress on tropical cyclone structure and intensity. *Trop. Cyclone Res. Rev.*, **1**, 254–275.

Zamudio, L., E. Metzger, and P. Hogan, 2010: Gulf of California response to Hurricane Juliette. *Ocean Modell.*, **33**, 20–32, doi:10.1016/j.ocemod.2009.11.005.

Zedler, S. E., 2009: Simulations of the ocean response to a hurricane: Nonlinear processes. *J. Phys. Oceanogr.*, **39**, 2618–2634, doi:10.1175/2009JPO4062.1.

Zhang, J. A., P. G. Black, J. R. French, and W. M. Drennan, 2008: First direct measurements of enthalpy flux in the hurricane boundary layer: The CBLAST results. *Geophys. Res. Lett.*, **35**, L14813, doi:10.1029/2008GL034374.